Detailed design of a forest surveillance UAV

Oleh Tkachuk
oleh.tkachuk@tecnico.ulisboa.pt

Instituto Superior Técnico, Universidade de Lisboa, Portugal

November 2018

Abstract

The aim of this work is to develop an Unmanned Aerial Vehicle (UAV) for fire surveillance by using an adequate, low-cost platform for high risk missions. This project, named DeltaSpotter, had a previously developed first working prototype, which in combination with a market research allowed for a better understanding of the characteristics necessary for an efficient long endurance UAV design. After detailed analysis of several possible configurations, the flying wing design was kept, as it was the most adequate for the mission requirements. Extensive research in regard to materials, methods of manufacturing and propulsion systems was completed, resulting in lower costs without compromising performance.

In addition, both size and shape of the UAV were defined. With the conceptual design completed, ensues the stability analysis and flight envelop of the design. This was followed by geometry modeling (by means of CAD software) and structural design (using a finite element software). To finish the design, the aerodynamic performance was studied, using CFD, which allowed for the calculation of a theoretical endurance value. The resulting DeltaSpotter aircraft has a two hour increase in endurance compared with the previous version. To finish the development process, several aspects of the drone's mission were described in detail.

Keywords: AM Plastic, Foam Core Airfoils, High Risk Missions, Low-Cost, UAV Design.

1. Introduction

In continental Portugal 39% of the territory is forest terrain, which translates into roughly 3,481 thousand hectares of land. When looking at reports exposing the impact of large fires in last 3 decades, it becomes transparent that the areas affected are similar year after year, showing a clear flaw in prevention and surveillance that needs to be addressed. To better understand the current methods of surveillance, several meetings were held with the Portuguese entities responsible for forest/fire surveillance and monitoring. During these meetings, several methods were discussed, covering their implementation, advantages and shortcomings. from their advantages and implementation to their shortcomings. The bulk of these efforts were said to rely substantially on monitoring from strategically placed watch-towers. However, these have a limited range of vigilance and only fully work after the first of July. This is clearly ineffective as before this period there is frequently heat waves across the country that exacerbate the probability and magnitude of either natural or man-manned fires. This method is complemented by GNR patrols that survey areas out of range from the towers and discourage possible arsonists or careless forest visitors. It was discovered that some entities possess highly technological drones. However, since these were very expensive acquisitions with complicated maintenance and highly specialized operators (pilots), they are mostly left unused due to fear of losing the equipment and initial investment.

With this information, engineers at Centre of Engineering and Product Development (CEiiA) set to develop an UAV that would be suitable for high risk missions (with high probability of loss of equipment). In addition, for the UAV to be implemented as a powerful tool of surveillance, it ought to be easy to carry and use without specialized training. The project, named DeltaSpotter, had a first prototype built in the summer of 2017 which served as a proof of concept and allowed for testing open source software and hardware. With mostly positive results, CEiiA gave the approval for the development of a long endurance version that should also correct the shortcomings of the first prototype, which will be the aim of this work.

2. Background

The design process of an UAV depends on the mission requirements. Since the UAV does not require a person inside, it opens up new possibilities for the use of design space and allows for more freedom

regarding the size, manufacturing techniques and materials. It also allows for the simplification of some systems and the removal of systematic redundancies. The materials in particular may be simpler, lighter and cheaper than those typically used in manned vehicles. This also means that new types of materials and manufacturing techniques can be tested and implemented such as foams, polymers and additive manufacturing. In fact, with novelty approaches for both material and manufacturing techniques, it became feasible to improve the performance of aerodynamic surfaces at a reduced cost, without compromising efficiency [1].

2.1. DeltaSpotter V1

Before starting the process of development for the long endurance version of DeltaSpotter, it is important to introduce the first prototype, DeltaSpotter V1, which was developed in cooperation with the aeronautical team at CEiiA during a Summer Internship Program. The author of this work accompanied the entire development process and participated in the decision making. This prototype was designed as a proof of concept, in order to understand if it was feasible to develop a low-cost fully autonomous platform for high risk missions, in this particular scenario to act as a fire detection system. Accordingly, the system was developed with only open source software (Mission Planner) and hardware (Autopilot 2.8). The main goal was to understand which features were required and to test the performance of Mission Planner and Autopilot. During the development, there was an effort to also analyze the market and present the project to possible customers. However, Computational Fluid Dynamic (CFD) and structural analyses were not performed, as this phase was still a proof of concept.

This prototype was built in order to be a low cost, lightweight model aircraft. As such, the wings were made of XPS foam, which has a high capacity to absorb impact, while the spar and central frame were built out of plywood. After the manufacturing process was complete, flying tests were successfully performed. Nevertheless, some issues were reported, such as a limited endurance time and complications with the autopilot leveling which was thought to be caused by the central frame, likely due to the plywood used in it.

After acknowledging and examining the triumphs and shortcomings of the first prototype, the aim is now to develop a new UAV for a longer endurance. As was the case with the previous version, the UAV must take off by hand launching, be low cost, easy to assemble and transport. With this last constrains in mind, the wing span should not exceed $3\,m$ as it will be transported by GNR patrols, in accordance to already implemented national surveillance strategies. The UAV should also be prepared to carry a payload of around $500\,g$ and withstand gusts around 30 to $40\,km/h$. Finally, an internal structure adequate to use in both V1 and V2 will be designed.

2.2. UAV configuration

As mentioned above, the configuration of the UAV depends on its intended mission. In this case, to survey and monitor large areas, an UAV with fixed wings (Conventional Take-Off and Landing, CTOL) would be more effective, as they have longer endurance and the ability to fly at much higher altitudes [1].

In order to choose the most adequate configuration, a decision matrix was employed, where four configurations (conventional configurations with tailplane-aft, canard configuration with a tailplane forward, tail-aft on booms and flying wing) were compared in accordance to the project requirements. It was concluded that the flying wing configuration is the most suitable configuration for this application, since it is easy to carry and has a low manufacturing price, without compromising the maneuverability and the aerodynamic efficiency.

2.3. Materials and Manufacturing Methods

The aircraft structure should be lightweight, to maximize endurance, while being stiff enough to bear the required loads. Moreover, a key factor in keeping the costs contained is the choice of materials and manufacturing techniques. In this particular case, only cost-effective materials will be analyzed, such as foams and polymers. Regarding the foams, they are inexpensive, easy to shape, repair and substitute, while also being lightweight and resistant to impact. This makes foams the ideal choice for wing manufacturing since it ensures a light weight component but does not compromise their shock resistance. For the manufacturing of the wing itself, a 4 axis hot wire cut will be used after airfoil selection and modelling.

The other material of particular relevance to ensure the development of a cost-effective UAV are polymers. These are usually known for a relatively low weight, resistance to corrosion and lack of conductivity (thermal and electrical). In addition, since they are easy to soften or melt when heated, and also become firm when cooled, making them ideal for heat dependent manufacturing techniques. In general, polymers have low prices due to being chemically mass produced from petroleum, although there have been significant investments in producing polymers from renewable sources (i.e. biofermentation of corn starch) to decrease the consumption and dependence of fossil fuels. The most common used polymer filaments include Acrylonitrile Butadiene Styrene (ABS), Polylactide (PLA),

Nylon, Polycarbonate (PC), and Polyvinyl Alcohol (PVA).

Recently, Additive Manufacturing (AM) has exploded in popularity due to the flexibility of building a component, layer by layer, based on a computer model. It is widely used to build prototypes and components with a small rate of production, providing fast prototyping and production of complex geometries. The type of AM technology used depends on the application and requirements. In this case, since CEiiA already owns a Fuse Deposition Modeling (FDM) printer, which is adequate to print the desired pieces, this will be the technique used. In doing so, new investments are avoided. The material to be used for the printing is PLA due its high tensile strength. In addition, it is biodegradable, recyclable and sourced from renewable sources, lowering the UAV's carbon foot print [2].

2.4. Propulsion System

Another key component of the UAV is the propulsion system, which provides the necessary power to propel the aircraft forward. The power from the propulsion system must be enough to balance the drag of the aircraft when it is in cruise mode and it must exceed the drag of the UAV for it to climb. There are several types of propulsion, but only two are commonly used in UAVs, the Internal Combustion engines and Electric Propulsion [1].

Internal Combustion engines use gasoline, methanol or diesel as fuel and are usually used in long-endurance aircraft. However, due to their small size, engines have numerous deficiencies: they are noisy; polluting; with a high thermal signature; and produce a lot of vibration, which requires reinforcements in the structure and frequent maintenance [3].

The Electric Propulsion uses an electric motor, which has a smaller number of parts when compared to an internal combustion engine, allowing an increase in engine revolutions. Its thrust can be controlled more precisely and it responds faster to throttle input due to the high torque available. In addition, it requires less maintenance, further lowering the cost. Taking into account that an electric motor practically does not have any movable parts when compared to an internal combustion engine, it allows an increase of the engine revolutions. Overall it also requires lower maintenance. From an economical point of view, the electric propulsion is less expensive. In addition, it is known to be quiet, without gas emissions and with low vibrations.

Another important factor to consider is that carrying rechargeable batteries is preferable to inflammable fuels as it reduces the chances of causing a fire, which in this case would defeat the project's purpose. Accordingly, an electric propulsion system was selected for this project.

3. Preliminary Design

In order to conceptualize an unmanned aerial vehicle, an iterative process is defined, which is presented in Figure 1.

The definition of the requirements and constraints, in collaboration with the Portuguese authorities, was based in the shortcomings of the first prototype and in extensive market research. With this finalized, the mission profile was designed and both the aircraft configuration and the propulsion system were chosen, thus obtaining a new conceptual design. At the end of this stage, in decision point D1, the results were analyzed in light of the requirements: if considered accurate enough, the process proceeds to the aerodynamic and structure detailed design; otherwise it returns to the requirements/constraints step.

A comprehensive design of the structure was carried out alongside the aerodynamic analyses. After completion, the resulting structural design's performance was evaluated (decision point D2): if judged accurate, the fabrication step initiates; otherwise the structural and external geometries designs are revised (to improve aerodynamics).

After building the DeltaSpotter V2 prototype, flight tests will be initiated.

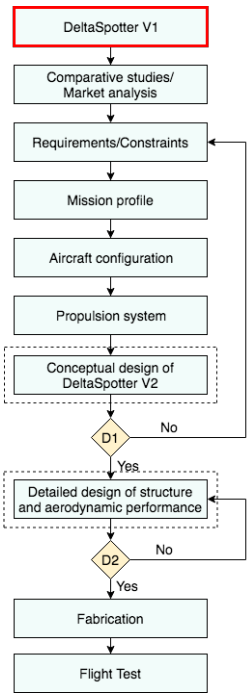

Figure 1: General Design Process.

3.1. Conceptual Design of DeltaSpotter V2

This section is related with the conceptual design of the platform which is an iterative process com-

posed of five steps (initial weight estimation, airfoil selection, wing configuration, stability analysis and flight envelope). To start, the initial sizing and weight estimation is performed in accordance to the first platform. To adapt to a long endurance UAV, it was considered that the battery would represent 50% to 60% of the total weight [4]. Accordingly, a weight estimation of $30\,N$ was considered.

In order to obtain a first estimation of endurance, the following equation for the electric propulsion is used,

$$T_E = \frac{E_T\,\eta_P}{\frac{1}{2}\,\rho\,U^3\,S(C_{Do} + \frac{1}{\pi\,AR\,e}(\frac{W}{\frac{1}{2}\rho\,U^2\,S})^2)} \quad (1)$$

where T_E is the endurance in hours, η_P is the propulsive efficiency, ρ is the air density, U is the speed of the UAV, C_{Do} is the zero lift drag, AR is the wing aspect ratio, e is the osvald factor, W is the weight of the UAV and S is the wing area.

3.2. Aerodynamics

For the aerodynamic analysis, an open source program named XFLR5 was used. Vortex Lattice Method (VLM) was selected for the wing analysis, as it was the most adequate for the shape of the wing.

Since the most important feature of an airfoil for a flying wing is a moment coefficient close to zero, only some airfoils are adequate. Based on published data [5], fourteen airfoils were selected and analyzed in order to obtain the airfoils with the highest value of C_L/C_D. These were analyzed at low Reynolds number ($5,000 < Re < 1,000,000$). From this analysis, five airfoils were selected and modified according to the thickness to chord ratio (t/c) and the thickness in the trailing edge, which must be $5\,mm$ (due to the manufacturing technique used).

Selected some potentials airfoils, the wing configuration ensues. The trapezoidal construction was chosen since it is simple to manufacture and has a relatively low root bending moment. For this type of wing, the taper ratio should be 40% (i.e. $\lambda = 0.4$) [6]. Another essential parameter to define is the sweep angle (Λ). The increment of this angle contributes for the directional stability [7], although a large value of sweep angle reduces the wing efficiency (C_L/C_D). Based on Ref. [8], an appropriate value for the sweep tailless UAVs is 15. Another selected parameter is the dihedral angle, which in this case will be 3°. This angle has a role during landing, as it causes the wing tip to stay above ground, allowing the UAV to perform softer landings. Knowing that the internal structure should be able to be used in both versions, the root chord and the thickness to chord ratio should be the same of the first prototype, meaning that $c_{root} = 500\,mm$ and $t/c_{root} = 14\%$. On the other hand the Aspect Ratio (AR) was restricted by the wingspan ($3\,m$) and the mean aerodynamic chord, resulting in a value of 8.57.

With the size and shape of the wing defined, the previously selected and modified airfoils (HS 522-MOD, MH45-MOD, MH 60-MOD MH 61-MOD and S5010-MOD) are applied to the wing models, which are then compared between each other. Comparing the results of C_L/C_D vs. speed (presented in Figure 2), C_L vs. angle of attack, moment coefficient vs. speed and the angle of attack vs speed, from each model, the MH 45-MOD airfoil was found to be the most adequate.

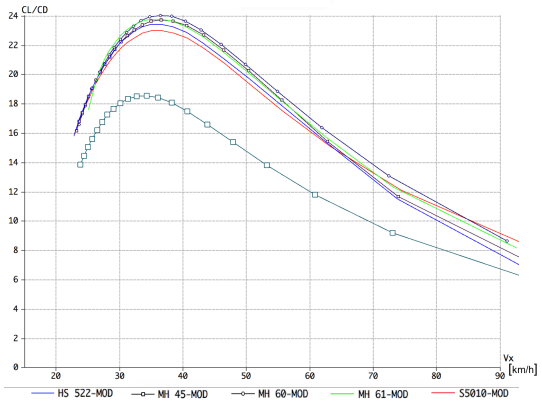

Figure 2: C_L/C_D vs. U_x.

This analysis allowed to adjust the incidence angle (2.5°) and the center of gravity ($CG = 280\,mm$) position in function of the cruise speed, which is $15m/s$. It is important to refer that the performed analyses were made considering an air density $\rho = 1.225\,kg/m^3$ and dynamic viscosity $\mu = 1.5 \cdot 10^{-5}\,Pa.s$. According to the performed analysis, Table 1 presents the main aerodynamic parameters.

Table 1: Performance parameters of DeltaSpotter V2 from XFLR5.

Data	Value
Maximum lift coefficient ($C_{L_{max}}$)	1.08
Maximum lift angle of attack [°] ($\alpha_{C_{Lmax}}$)	10.5
Maximum lift-to-drag ratio ($(C_L/C_D)_{max}$)	23.7
Lift VS angle of attack curve slope [deg^{-1}] (C_{L_α})	0.078
Zero lift drag coefficient for cruise ($C_{D_{O_{cruise}}}$)	0.0097
Drag coefficient for cruise ($C_{D_{cruise}}$)	0.011
Lift coefficient for cruise ($C_{L_{cruise}}$)	0.20
Lift-to-drag ratio for cruise ($(C_L/C_D)_{cruise}$)	17.82

With the size and shape of the UAV defined, the choice of electronic components ensues:

- Autopilot 2.8 + GPS + Radio Wireless Telemetry + Power module;
- Battery 4S, 5 Ah;
- Control Actuators;
- Electric Motor + Propeller 12x6 (Max thrust: 2300g);

- Electronic Speed Controller (ESC) 60A;

Regarding the weight of the aircraft, the estimation was kept on 30 N, where the batteries represent 1.4 kg. Three batteries are used and connected in parallel, each one of them has a 4S configuration with the capacity of 5 Ah.

3.3. Stability Analysis

The stability is a property of an equilibrium state. As such, if an aircraft keeps in a steady uniform flight the resultant forces and moments in relation to the center of gravity must be zero. Thus, when this condition is satisfied, the aircraft is in a state of equilibrium which may be called trimmed flight. Stability is the capacity of the aircraft to keep the trimmed flight condition and restore it when it is affected by perturbations like force or moment. This can be divided in static and dynamic.

The aircraft is statically stable when it tends to restore to its original position (orientation and speed). In order to evaluate the static stability, the longitudinal and lateral derivatives are analyzed and compared with the conditions of stability. In conclusion, both longitudinal and lateral motions are stable.

The dynamic stability is based on the time history of the aircraft motion after some perturbation. An aircraft may be statically stable but dynamically unstable. It is considered that the aircraft is dynamically stable whenever the amplitude of any oscillatory motion induced by some perturbation decreases to zero relatively to the steady state flight condition. Thus, dynamic stability is the reduction of the disturbance in time, which means that there is energy dissipation, called positive damping (works against perturbation).

Therefore, in order to study the dynamic stability, differential equations must be analyzed. Regarding small perturbations, these can be decomposed into longitudinal and lateral directions, obtaining the eigenvalues, the respective natural frequency and the damping ratio. From the eigenvalues, it is concluded that, excluding the spiral mode, all others are stable. This is unsurprising as the spiral mode is usually unstable.

The eigenvalues obtained are compared with the flying qualities required by MIL-F-8785C. It was concluded that the flying qualities are clearly adequate for the mission flight phase (non-terminal flight phases that are normally accomplished using gradual maneuvers).

3.4. Flight Envelope

In order to define the configuration of the UAV and the reinforcements it should have, all the loads that aircraft would be subjected during its operation life would ideally need to be well described. Since this is not feasible, only the most critical cases are analyzed. In order to define the maximum load factors that can be expected for an UAV, STANAG 4703 norm [9] is used. This is destined for the certification of a fixed-wing light Unmanned Aerial System (UAS) with a maximum take-off weight not greater than 150 kg. This standard allows to design the maneuver V-n diagram, which is presented in Figure 3 for standard sea level.

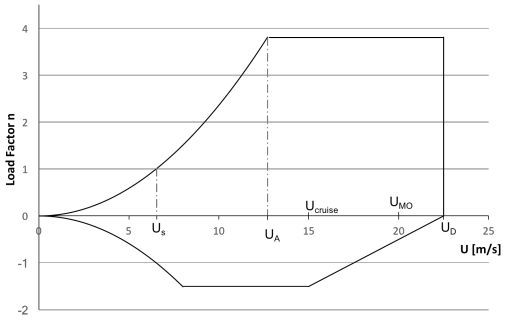

Figure 3: Maneuver V-n diagram of the DeltaSpotter V2 for standard sea level.

Where the stall speed (U_s) is 6.5 m/s, the maneuver seed (U_A) is 12.7 m/s and the dive speed (U_D) is 22.5 m/s.

Since the atmosphere is considered a dynamic system, gusts are to be expected during flight. When it occurs, the angle of attack changes, which means that the lift force is affected and consequently the load factor as well. Typically, the gust velocity $\hat{u}$ is obtained from statistical flight data, when considering the altitude range and flight conditions. According to STANAG 4703 norm, between sea level and 6096 m, the positive and negative gust values to consider should be 15.2 m/s at cruise speed and 7.6 m/s at maximum operational speed, this should be no more than 90% of the dive speed, thus $V_{MO} = 20.25\,m/s$. The load factors for both velocities are then calculated, which result in $n = +8.1$ and $n- = -6.1$ for cruise speed and $n+ = +5.8$ and $n- = -3.8$ for maximum operating speed. The gust envelope is drawn and combined with the flight envelop (maneuver V-n diagram), as seen in Figure 4 [6].

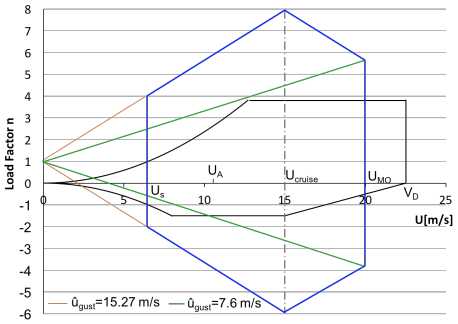

Figure 4: Combination of maneuver V-n diagram with the load factors induced by the gusts.

The gust values given by STANAG 4703, are highly conservative. However, due to the fact that this UAV is designed for high risk missions, it is expected that it should be prepared for adverse weather conditions. Accordingly, the largest values will be used in the structural design. Figure 4 shows that for high values of gust, the gust envelop has a higher load factor than the flight envelop. In this scenario, the aircraft stalls. However, due to the fact that the autopilot controls the UAV, this can be avoided by changing the angle of attack and the velocity.

4. Structural Design and Analysis

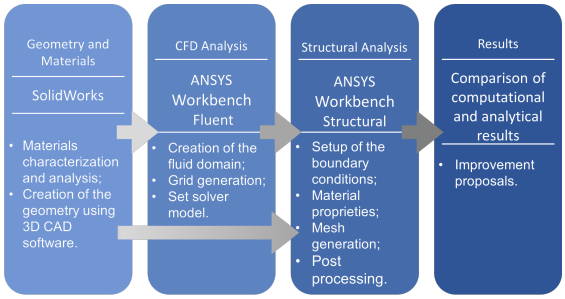

Figure 5: Flowchart with the various steps of structural design and aerodynamic analysis performed during wing design.

As shown in the flowchart above (Figure 5), the first step of structural design is the characterization of the materials and creation of a 3D Computer Aided Design (CAD) model, using the software SolidWorks© 2016. In this stage, the wing and its internal structure are created. With the CAD model finished, it is then imported to ANSYS®. The model will be used for CFD and Structural analyses. The CFD analysis is performed first, using ANSYS Fluent®, in order to obtain the loads required for the Structural analysis. ANSYS has a feature within Workbench that allows the coupling of both systems, CFD and Structural. Thus, the aerodynamic forces obtained in CFD are transferred to the structural analysis, simulating a wing load close to the real value. Finally, a comparison is made between the computational and analytical values, which allows further verification of any mistake in the used methods.

4.1. Material Analysis

As mentioned before, the wing will be made with XPS foam, which lacks a universal data sheet due to batch variability. This means that there are some technical characteristics missing that need to be calculated. The foam density was determined to be $\rho_{XPS} = 34.296\,kg/m^3$. In order to obtain the values of the Young's Modulus and the Tensile Yield Stress, a cantilever beam bending test was performed. The result can be found in Table 2.

PLA is also used for the wing construction, specifically for the internal structure, with FDM used for manufacturing. Most of the FDM parts are not printed solid, since it would require large amounts of material and a longer printing time, resulting in higher costs. To avoid this, different parameters like infill density, extrusion temperature, raster angle and layer thickness were analyzed. The combination that allows to reduce the costs, weight, manufacturing time, while maintaining a high yield resistance was chosen. The obtained parameters are: infill density of 40%, extrusion temperature of 220^oC, raster angle of $0/90^o$, and layer thickness of $0.2\,mm$ [2]. The material proprieties of PLA are defined in Table 2.

Table 2: Resume of the material proprieties.

	XPS	**PLA**
Young's Modulus $[GPa]$	0.01663	1.19
Yield Tensile Strength $[MPa]$	0.361	20.07

4.1.1 Geometry Modeling

This subsection describes the internal structure of the UAV, which is the physical support for the motor and all of the electronic components. In addition, because of its configuration (flying wing) it should also facilitate the UAV launch (by using the central frame).

Figure 6 shows the isometric view of the designed structure. This includes the main components: batteries (yellow), control actuators (pink), autopilot (bright green) and motor (black).

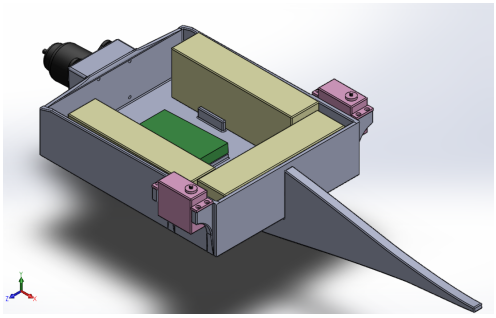

Figure 6: Isometric view of the internal structure.

The internal structure was designed to consider the dimensions of the electronic components, while simplifications were made in order to facilitate the printing process and reduce the printing time. The structure is divided in two parts, which are manufactured separately: the box (with the wall thickness of $4\,mm$) and the central frame, with a thickness of $10\,mm$. Additionally, in order to reduce the warping and the stress concentrations, all structure edges have a fillet of $1\,mm$.

Figure 7 shows a model of the full wing, with the vertical stabilizers, internal structure, and the main electric components.

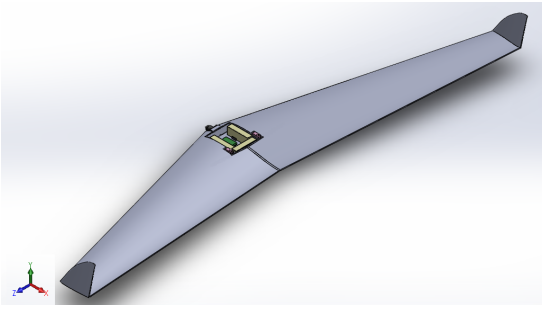

Figure 7: Isometric view of the wing.

4.2. CFD Analysis

The main goal of this subsection is to obtain the aerodynamic loads applied to the wing through a CFD analysis, and then use them for the structural analysis. Furthermore, this analysis allows for a comparison between the results of lift and drag obtained from XFLR5. The software used for the CFD analysis is ANSYS Fluent® 18.2 student version, with a limitation of $5.12e5$ nodes/cell. As such, to reduce the computational time, only half of the wing is analyzed, thus taking advantage of the wing symmetry. To further simplify it, the vertical stabilizers will be excluded from the analysis. A CAD model of the wing is used in order to delimit the shape of the interface between object and fluid. The next step is to model the control volume (fluid domain), which should be large enough to minimize the numerical error, due to the boundary conditions in the proximity of the geometry.

In order to solve the CFD analysis, it is crucial to choose a turbulence model, which will predict its evolution. The velocity and pressure of a fluid flow is governed by Navier-Stokes equations, where the instantaneous quantity is decomposed into a mean part and a fluctuating part. Due to the fact that there are no exact solutions for these equations, the Reynolds-Averaged Navier-Stokes (RANS) equations are used, giving approximate time-averaged solutions to the Navier-Stokes equations.

The choice of the model depends on the application, the level of accuracy required, available computational resources, and the amount of time available for the simulation. For this simulation, the chosen model was the Standard $k-\epsilon$. This is the most widely-used engineering turbulence model for industrial applications in CFD analysis. It is also known to be robust, economic, and reasonably accurate for a wide range of turbulent flows.

In order to better predict fluid behavior, in the boundary layers near the solid wall, prism layers are used [10]. The parameter y^+ is used in order to define the thickness of the first prism layer, defining also a growth rate for the remaining layers. This parameter is used to define how coarse or fine a mesh is, in a first layer. For turbulent analysis, using a $k-\epsilon$ models, it is recommended values of $30 < y^+ < 300$. Thus, $y^+ = 50$ is used in this analysis. When considering other parameters like velocity, air density, air viscosity, mean chord and flow type, the first layer thickness is obtained, $1.75\,mm$. This parameter is used in the inflation layer in order to accurately capture the boundary effects of the flow around the wing.

The next step of the analysis is to define the flow boundary conditions. The inlet velocity is imposed with $15\,m/s$. The outlet wall was defined as the pressure-far-field. The other side of the flow was defined with symmetry.

After choosing a model, defining the y^+ value and boundary conditions, the grid generation ensues. A hybrid grid is used, where the main elements are tetrahedral (and, in the solid wall, hexahedral elements are used). Additionally, in order to obtain better resolution in the wing a rectangular block around it is used.

It is intended that the results do not change with mesh refinement. With this in mind, a convergence analysis is performed, by presenting the lift and drag forces as a function of the number of elements, as shown in Figure 8. Between each iteration, a reduction of the element size is calculated, increasing the number of elements.

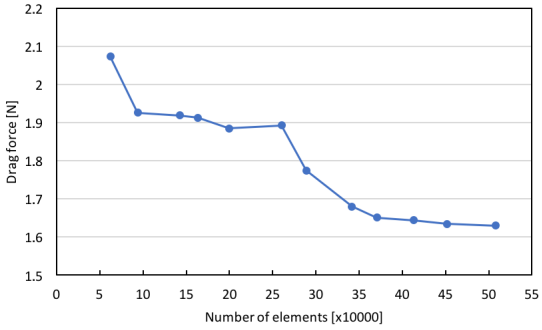

Figure 8: Results of drag analysis in function of the number of elements.

Figure 8 shows that from the $3.7 \cdot 10^5$ element, the drag force stabilizes. Consequently, $3.7 \cdot 10^5$ numbers of elements are enough to obtain accurate results with minimum computational effort.

After solving all iterations, the convergence of the residual sum is verified. Thus, with values of energy, k and ϵ in the recommended range, the result analyses ensues.

Table 3 presents the lift and drag coefficients obtained from ANSYS Fluent:

Table 3: Lift and drag coefficients from Fluent.

Data		Value
Lift coefficient for cruise	$C_{L_{cruise}}$	0.203
Drag coefficient for cruise	$C_{D_{cruise}}$	0.0225
Zero lift drag coefficient for cruise	$C_{D_{0_{cruise}}}$	0.0102
Induced drag coefficient for cruise	$C_{D_{i_{cruise}}}$	0.0124

In order to compare the result between both used software, Table 4 is presented, where it is also shown the error as a function of the values obtained from Fluent.

Table 4: Comparison between results obtained from XFLR5 and Fluent.

	XFLR5	**Fluent**	***%error***
Lift [N]	29.375	29.379	0.01
Drag [N]	1.628	3.301	50.68
Endurance [h]	6.4	3.23	115.5

It is possible to observe that the values presented in Table 4 are similar in terms of lift force and different in terms of drag force, as expected. According to the literature, XFLR5 gives a good estimation of lift, but tends to underestimate the drag. Consequently, since one of the variables for the endurance calculation is the drag force, the endurance time calculated using data from XFLR5 was overestimated, due to the fact that these parameters have an inverse relation.

Figure 9 presents velocity distribution around the wing.

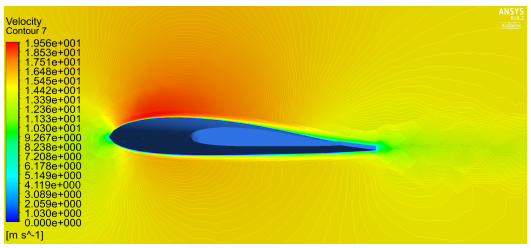

Figure 9: Representation of the velocity around the wing.

With the previous results verified, the forces obtained in this subsection can now be used for the structural analysis.

4.3. Structural Analysis

Prior to the computational analysis, analytical calculations should be performed in order to have an idea about the order of magnitude of deflection and maximum stress. This would allow the comparison between the values obtained from both methods, and verification of possible errors in the models. In order to simplify the system, the wing was approximated to a cantilever beam with a constant cross section. Additionally, the lift force was approximated as a constant distributed force ($q = 9.793\,N/m$). The maximum deformation of the beam is calculated as follows: 2.

$$I = \frac{w\,i^3}{12} \qquad y_{max} = -\frac{q\,l^4}{8\,E\,I} \tag{2}$$

where, I is the moment of inertia, w is the width of the beam, i is the height, q is a constant distributed force, l is the length of the unclamped beam, and E is the Young's Modulus. The value of the maximum deformation, at the free end, is $427.988\,mm$. Moreover, by applying the equations of pure bending theory [11], the maximum stress is calculated:

$$\sigma_{max} = \frac{M\,y}{I}; \qquad y = i/2. \tag{3}$$

Due to the fact that the maximum stress occurs at the root of the wing, a new moment of inertia is obtained for this cross section. According to this, the obtained maximum stress is $\sigma_{max} = 65003\,Pa$. With the analytical analysis concluded, the computational analysis ensues.

4.4. Computational Structural Analysis

This analysis uses the Finite Element Method (FEM), where the geometrically complex domain of the structural problem is systematically represented by a large, but finite, collection of simpler sub-domains, called finite elements. The polynomials are used in order to approximate the displacement field of each element. These are interpolated with respect to the preselected nodes and are referred to as interpolations, where different methods can be applied in order to determine the unknown nodal values (displacements). In function of these nodal values, stresses and strains are determined [12].

The structure is expected to always be under elastic deformation, which means a linear analysis is enough to characterize it [12]. A linear static analysis means that load conditions do not vary in time. It also assumes that the small deflection theory is taken into consideration, and that the materials have linear elastic behavior.

Firstly, the material proprieties are defined. The definition of the boundary conditions follows. In order to constrain the wing, where a fixed support is used on the root face. This restrains all of the six degrees of freedom, translation and rotations in x, y and z directions. Thus, the forces that are applied on the wing are descendant from the coupling system of the fluid-solid interface.

Due to the fact that the wing is a 3D solid, a solid 3D element should be used, in this case SOLID 186, which is a second order element, defined by 20 nodes with three degrees of freedom per node: translations in the x, y, and z directions. With the element type defined, the mesh is generated. As with the CFD analysis, a mesh convergence study was also made

for maximum deformation, maximum Von Misses stress (Figure 10), maximum and minimum principal stresses. The results converged after 3780 elements (20511 nodes).

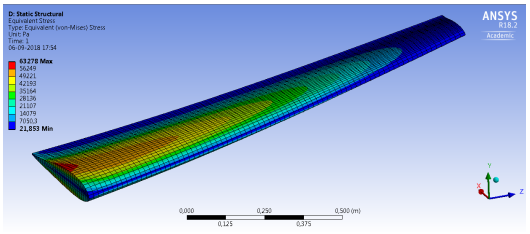

Figure 10: Equivalent Von-Mises Stress for cruise speed.

Therefore, the maximum wing deformation is $106.7\,mm$ obtained at the tip of the wing, and the maximum stress is $|-63.563\,kPa|$ corresponding to the minimum principal stress. These values have the same order of magnitude when compared to analytical values, which gives confidence in the validity of the obtained results. Knowing that the aircraft must withstand the gusts previously defined, the load factor of $n = 8.1$ is applied,

$$\sigma_{max} \times n_{max} = 514.860\,kPa > \sigma_{yield_{XPS}}. \quad (4)$$

It is important to refer that this consideration is made, due to the fact that the structure is in elastic deformation. Moreover, this is a simplified method making this a conservative approach.

Since the maximum stress is clearly higher than the maximum yield stress, the wing requires a reinforcement. Thus, the spar is created using the same material of the internal structure (PLA). This reinforcement will be attached to the back side of the frame in a perpendicular direction to the root face, in order to support the most critical areas.

A new analysis is performed with the reinforcement. Taking into account that there are two structures (wing and reinforcement), it is essential to define the type of connection created, which is bonded, preventing sliding or separation between faces. To do so, two types of elements are used, TARGE170 and CONTA174. A new mesh is also made, where the reinforcement is meshed with element SOLID186 and the wing is meshed with element SOLID187. Due to the geometry and the constraint of the number of nodes/elements, it was not possible to use element SOLID186 for the wing.

Comparing both analyses, it is possible to verify that the maximum wing deformation was reduced from $107\,mm$ to $26\,mm$ for cruise speed. This was expected since PLA has an increased stiffness.

Beyond the deformation, the stress is also analyzed. With the reinforcement, the average stress in the wing is low (around $20\,kPa$), most of the loads are supported by the reinforcement, which due to its material proprieties can withstand a maximum load factor of $n = 8.1$. Figure 11 presents the Von-Mises stress of the wing near to the reinforcement.

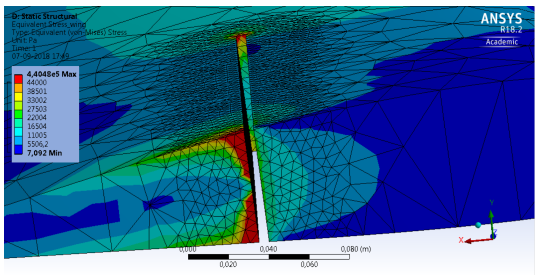

Figure 11: Representation of Von-Mises stress distribution in the wing.

From Figure 11 it is observable that there are three regions with stress concentration. These areas are near to abrupt changes in geometry which disrupt the smooth flow of stress through the structure. This induces large stress gradients, where the maximum stress greatly exceeds the average and normal values. In order to fix the stress concentration, the recommended procedure is to smooth the edges. This can be made with the increment of the radius of the edge [12]. Due to the fact that the red zones are stress concentrations, induced by the shape, these values should be ignored for the structural analysis.

To summarize, the internal structural design was completed and shown to be adequate for both prototypes (long and short endurance). The wing performance was validated and, if necessary, reinforcements could be used as it happens in V2. In addition, the design of the aircraft respects STANAG 4703 norm, which is crucial for its functionality.

4.5. Mission

This subsection has the main goal of giving an overview of the necessary steps to put and keep the aircraft in flight, the missions that the UAV can perform and the area that it can survey without changing batteries. Before describing the launching process, it is crucial to keep in mind that the main ambition of this project is to have a fully autonomous system, which allows to reduce costs with operator training. In this regard, the training involved would only be related to the mission planning and the launching of the UAV. For the accomplishment of a mission it is necessary to have two operators, one to give the order to start the mission in the software, and another to perform the launching.

For the accomplishment of the mission, it is just required the connection of the batteries to the system. Regarding the mission generation, the area to survey must be defined at the ground station (which could be a portable computer). Additionally, some parameters must be introduced i.e. cruise speed,

flight altitude and the distance between each passage line, and the mission is automatically generated. The distance between each passage depends on the camera that is used and the flight altitude.

As an example, flying at 200 m of altitude, with a distance of 700 m between each passage (illustrated in Figure 12) it is possible to survey an area of 7,966 ha, requiring around two and a half hours.

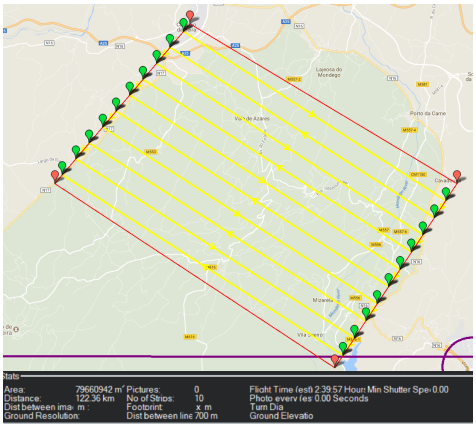

Figure 12: Representation of the mission simulation.

5. Conclusions

This document summarizes the design of a new prototype of the DeltaSpotter with a longer flight period. Due to its fire-surveillance purpose this design had several constraints in order to be useful on a large-scale surveillance methodology.

The resulting UAV has a theoretical endurance between two and a half hours and three hours (these values were obtained considering a margin of 10% and 20% of total battery charge for takeoff, climb and remaining battery charge), which corresponds to an improvement of 1.5 to 2 hours in regard to the previous prototype. The size and configuration of the aircraft is adequate to make it easy to carry (3 m of wingspan) and to be hand launched. The manufacturing cost was calculated by adding the cost of the materials (XPS and PLA, 30 € and 15 € respectively) to the electric components. Consequently, the total cost of materials and components adds up to 300 €, a fraction of the price of most surveillance UAVs available in the market.

It is worth to notice that these analyses were done with a computational limitations in term of the number of cells/elements. This clearly constrains the analysis, since in this simulation the vertical stabilizer was not included in the CFD and structural analysis. In addition, the number of elements restricted the reinforced wing analysis. Nevertheless, the simulation was completed with a fully defined wing and internal structure that follow the requirements and the norm STANAG 4703, which itself is quite restrictive.

At this time, the prototype has not yet been manufactured, although completion is expected to be reached until the end of October, where several flight tests are expected to be performed, to guarantee structural integrity and obtain real endurance times.

References

[1] D. M. Marshall, R. K. Barnhart, E. Shappee, and M.T. Most. *Introduction to Unmanned Aircraft Systems, Second Edition*. CRC Press, 2016.

[2] J. F. M. Fernandes. Estudo da Influência de Parâmetros de Impressão 3D nas Propriedades Mecânicas do PLA. Master's thesis, UL - Instituto Superior Técnico, October 2016.

[3] A. J. Keane, A. Sóbester, and J. P. Scanlan. *Small Unmanned Fixed-wing Aircraft Design: A Practical Approach*. Wiley, 2017.

[4] T. Chang and H. Yu. Improving electric powered uavs' endurance by incorporating battery dumping concept. *Procedia Engineering*, 99:168–179, 2015.

[5] P. Edi, N. Yusoff, and A. A. Yazid. Airfoil design for flying wing uav. *WSEAS Press*, pages 106–111, 2008.

[6] T. C. Corke. *Design of Aircraft*. Prentice Hal, 2003.

[7] R. Austin. *Unmanned Aircraft Systems*. Wiley, 2010.

[8] J Hall, K Mohseni, and D Lawrence. Investigation of variable wing-sweep for applications in micro air vehicles. *AIAA Journal*, (September):26–29, 2005.

[9] NATO Standard AEP-83 Light Unmanned Aircraft Systems Airworthiness Requirements, STANAG 4703. *NATO Standard AEP-83*, 2014.

[10] J. H. Ferziger and M. Peric. *Computational Methods for Fluid Dynamics*. Springer, 2002.

[11] F. P. Beer, E. R. Johnston, J. T. DeWolf, and D. F. Mazurek. *Mechanics of Materials*. Mc Graw Hill, 2015.

[12] W. C. Young and R. G. Budynas. *Roark's Formulas for Stress and Strain*. Mc Graw Hill, 2002.